HIGH PRESSURE SHOCK WAVE BEHAVIOR OF GREATLY DISTENDED COPPER

F. H. Shipman, et al

General Motors Technical Center

Prepared for:

Ballistic Research Laboratories

December 1972

BRL CR 84

BRL

AD

CONTRACT REPORT NO. 84

HIGH PRESSURE SHOCK WAVE BEHAVIOR OF GREATLY DISTENDED COPPER

Prepared by

Materials and Structures Laboratory
General Motors Corporation
Warren, Michigan

December 1972

USA BALLISTIC RESEARCH LABORATORIES
ABERDEEN PROVING GROUND, MARYLAND

62

When this report is no longer needed, Department of the Army organizations will destroy it in accordance with the procedures given in AR 380-5. Navy and Air Force elements will destroy it in accordance with applicable directives. Department of Defense contractors will destroy the report according to the requirements of Section 14 of the Industrial Security Manual for Safeguarding Classified Information. All others will return the report to Commanding Officer, U.S. Army Aberdeen Research and Development Center, Aberdeen Proving Ground, Maryland.

Secondary distribution of this report by originating or sponsoring activity is prohibited.

Additional copies of this report may be obtained from the Defense Documentation Center, Cameron Station, Alexandria, Virginia 22314

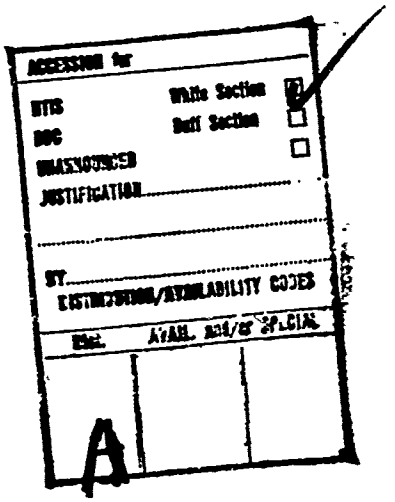

The findings in this report are not to be construed as an official Department of the Army position, unless so designated by other authorized documents.

BALLISTIC RESEARCH LABORATORIES

CONTRACT REPORT NO. 84

DECEMBER 1972

HIGH PRESSURE SHOCK WAVE BEHAVIOR OF GREATLY DISTENDED COPPER

F. H. Shipman
A. R. McMillan

Materials and Structures Laboratory
Manufacturing Development, General Motors Corporation
General Motors Technical Center, Warren, Michigan 48090

Contract No. DAAD05-71-C-0403

ABERDEEN PROVING GROUND, MARYLAND

ABSTRACT

High pressure shock waves were studied in porous copper samples. These waves were induced by high velocity impact of flat plates. Flat plates of copper and a tungsten alloy were projected at velocities up to 8 mm/μsec using a two-stage light gas gun. Samples of porous copper with distention ratios of 3.08, 4.46 and 8.74 (32.4%, 22.4% and 11.4% of solid density) were studied through shock transit measurements. Analysis of the experiments reveals that a complex (two-wave) shock structure exists in the open celled materials impacted at conditions that would result in shock stresses up to 4 Mb in solid targets. The nature of the double wave precludes the use of the Rankine-Hugoniot equations which assume that thermodynamic equilibrium is attained behind a discontinuous shock.

UNCLASSIFIED

Security Classification

DOCUMENT CONTROL DATA - R & D

(Security classification of title, body of abstract and indexing annotation must be entered when the overall report is classified)

1. ORIGINATING ACTIVITY (Corporate author) Materials and Structures Laboratory Manufacturing Development General Motors Corporation, Warren Michigan	2a. REPORT SECURITY CLASSIFICATION UNCLASSIFIED 2b. GROUP

3. REPORT TITLE

HIGH PRESSURE SHOCK WAVE BEHAVIOR OF GREATLY DISTENDED COPPER

4. DESCRIPTIVE NOTES (Type of report and inclusive dates)

5. AUTHOR(S) (First name, middle initial, last name)

F. H. Shipman and A. R. McMillan

6. REPORT DATE	7a. TOTAL NO. OF PAGES	7b. NO. OF REFS
DECEMBER 1972	57	11

8a. CONTRACT OR GRANT NO. DAAD05-71-C-0403 b. PROJECT NO. c. d.	9a. ORIGINATOR'S REPORT NUMBER(S) MSL 71-30 9b. OTHER REPORT NO(S) (Any other numbers that may be assigned this report) BRL CONTRACT REPORT NO. 84

10. DISTRIBUTION STATEMENT

Approved for public release; distribution unlimited.

11. SUPPLEMENTARY NOTES	12. SPONSORING MILITARY ACTIVITY
	U. S. Ballistic Rsch Laboratories Aberdeen Proving Ground, Md. 21005

13. ABSTRACT

High pressure shock waves were produced and studied in porous copper samples by high velocity impact of flat plates. Flat plates of copper and tungsten alloy were projected at velocities up to 8 mm/μsec using a two-stage light gas gun. Samples of porous copper with distention ratios of 3.08, 4.46 and 8.74 (32.4%, 22.4% and 11.4% of solid density) were studied through shock transit measurements. Analysis of the experiments reveals that a complex (two-wave) shock structure exists in the open called materials impacted at conditions that would result in shock stresses up to 4 Mb in solid targets. The nature of the double wave precludes the use of the Rankine-Hugoniot equations which assume that thermodynamic equilibrium is attained behind a discontinuous shock.

Details of illustrations in this document may be better studied on microfiche

IR

DD FORM 1 NOV 68 1473 REPLACES DD FORM 1473, 1 JAN 64, WHICH IS OBSOLETE FOR ARMY USE.

UNCLASSIFIED

Security Classification

14. KEY WORDS	LINK A		LINK B		LINK C	
	ROLE	WT	ROLE	WT	ROLE	WT
Equation of state Highly porous copper High pressure shock waves						

TABLE OF CONTENTS

LIST OF ILLUSTRATIONS

LIST OF TABLES

SECTION I

INTRODUCTION

This report describes work performed by the Materials and Structures Laboratory of Manufacturing Development, General Motors Corporation, under Contract No. DAAD05-71-C-0403 monitored by the U.S. Army, Aberdeen Research and Development Center, Aberdeen Proving Grounds, Maryland. The purpose of this contract was to determine experimentally the Hugoniot equation of state of highly porous copper.

There are two areas of interest surrounding the shock compression of porous materials. As absorbers of mechanical energy porous materials combine the desirable qualities of good mechanical dissipation through large strains at low stresses and light weight. Secondly, insights into the physics of materials at high pressures and temperatures may be obtained through the study of shock compression of porous solids.

Many studies of the dynamic response of porous metals to suddenly applied loads have been performed in the low stress regime up to about 50 kb. Additionally, a good deal of experimental work [1,2,3,4,5] has been performed with metal foams or loosely packed powders at high pressures.

Theoretical descriptions of the shock propagation in porous solids are represented by the work of Thouvenin,[6] Butcher[4] and Kormer, et al.[1,2] Thouvenin represents the porous solid in a one dimensional sense as a series of plates and

voids (plate-gap model). The disturbance or shock is transmitted through the material by shocks through the solid plates and by the material crossing the gaps at the free surface velocity corresponding to the pressure state in the solid plate. Butcher[4] has described the porous solid in the same fashion but has restricted his application to low stress regimes.

The Russian workers, Kormer, et al.,[1,2] and Krupnikov, et al.,[3] have employed their very high dynamic pressure technology to porous metals and have therewith constructed equations of state for these metals that describes off-Hugoniot behavior.

The basic approach taken by the Russian workers has been to assume an equation of state of the general form:

$$P = P_c + P_\ell + P_e \qquad \text{and} \qquad (1)$$

$$E = E_c + E_\ell + E_e \qquad (2)$$

Where the subscript $_c$ denotes the 0°K isotherm and ℓ and e are thermal components arising from the lattice and electron contributions respectively. Determination of the 0°K isotherm is described by Kormer, et al.[1] This isotherm P_c (σ) at 0°K is believed to be valid over the entire volume range from a highly compressed solid in the Thomas-Fermi-Dirac regime to "cold ideal gas" states. The equation

$$P_c(\sigma) = \sum_{i=1}^{7} a_i \sigma^{(\frac{i}{3} + 1)} \qquad (3)$$

is used by references 1, 2, and 3, where the coefficients, a_i are determined by such constraints as the heat of vaporization,

bulk modulus, second and third order elastic constants, the shock-determined Grüneisen ratio, and the Thomas-Fermi-Dirac theory. Sigma, σ, is the state of compression or ρ/ρ_o. The cold compression curve P_c (σ) together with the lattice P_ℓ (σ,T) and the electron P_e (σ,T) temperature contributions is used to map states for copper in P, V, E or T thermodynamic planes.

To provide the equation of state with a large enough range an interpolation is required for the lattice terms. The equations:

$$P_{T_\ell} = \frac{3\gamma + Z}{1 + Z} \rho R \ (T-\hat{T}) \tag{4}$$

$$E_{T_\ell} = \frac{2 + Z}{1 + Z} \ \frac{3}{2} \ R \ \ (T-\hat{T}) \tag{5}$$

$$C_v = \frac{3}{2} R \ \left[1 + (1 + Z)^{-2}\right] \tag{6}$$

$$\lambda_\ell = \frac{2}{3} \frac{(3\gamma + Z)}{(2 + Z)} \tag{7}$$

are chosen where

$$Z = LRT/C_c^2 \qquad \text{and} \tag{8}$$

$$C_c^{\ 2} = \frac{dP_c}{d\rho} \tag{9}$$

is the sound speed along the 0°K isotherm. L is an experimentally determined constant, R is the universal gas constant.

$$\hat{T} = T_o - E_o/3R \tag{10}$$

where

$$E_o = \int_0^{T_o} C_v dT \qquad \text{and} \qquad (11)$$

$T_o = 300°K$.

As the parameter $Z \to 0$ equations (4) and (5) reduce to the Mie-Grüneisen equation:

$$P - P_c = \gamma\rho\,(E-E_c) \qquad (12)$$

Similarly:

$C_v = 3R$ and $\lambda_\ell = \gamma$ the Grüneisen ratio.

The functional form of γ used throughout is:

$$\gamma = \frac{1}{3} + \frac{\sigma}{2}\frac{d^2P_c/d\sigma^2}{dP_c/d\sigma} \qquad (13)$$

As $Z \to \infty$:

$P = \rho RT$, $C_v = \frac{3}{2}R$, $\lambda_\ell = \frac{2}{3}$, i.e. the ideal gas values.

For the electron terms an approximation to the Thomas-Fermi model is used which includes the electronic specific heat, $\beta(\sigma)$.

$$P_{T_e} = g\rho\frac{b^2}{\beta}\ln\cosh\left(\frac{\beta T}{b}\right) \qquad \text{and} \qquad (14)$$

$$E_{T_e} = \frac{b^2}{\beta}\ln\cosh\left(\frac{\beta T}{b}\right) \qquad (15)$$

where

$$g = - \frac{d \ln \beta}{d \ln \rho} \qquad \text{or} \qquad (16)$$

$$\beta = \beta_o / \sigma^g \qquad (17)$$

The experimental results from the porous work are used to establish values for g and L (which are assumed constants). Values for β_o and ρ_c are found from measurements near absolute zero temperatures. Putting these terms together then we have:

$$P = P_c(\rho) + \frac{3\gamma(\rho) + Z(\rho,T)}{1 + Z(\rho,T)} \rho R(T-\hat{T}) + g\rho \frac{b^2}{\beta(\rho)} \ln \cosh \left(\frac{\beta(\rho)\, T}{b}\right) \qquad (18)$$

$$E = E_c(\rho) + \frac{2 + Z(\rho,T)}{1 + Z(\rho,T)} \frac{3}{2} R (T-\hat{T}) + \frac{b^2}{\beta(\rho)} \ln \cosh \left(\frac{\beta(e)\, T}{b}\right) \qquad (19)$$

The procedure we used to determine Hugoniots is as follows. Equations 18 and 19 are not solvable for T, so by selecting a series of temperatures a family of isotherms was calculated over a range of values from V = 0.05 to 0.3 cm^3/gm. The pressure and specific energies for each volume state along each isotherm were plotted. Next a family of straight lines representing E/P ratios allowed by the Hugoniot equation:

$$\Delta E = E - E_o = \frac{1}{2} P (mV_o - V) \qquad (20)$$

where drawn in the E - P plane. Here $m = \rho_c/\rho_{oo}$, ρ_{oo} = porous density, $V_o = \frac{1}{\rho_c}$ and V is the shock state on the Hugoniot. In determing E/P only V is allowed to vary over the range of interest for each value of m. Thus the intersection of E/P (at some V_i) with the line along that same V_i through the various isotherms uniquely establishes the pressure, energy and temperature conditions for the Hugoniot state. This method, though graphical, gives quite good agreement with the data reported by Kormer et al.[1]

A listing of the computer routine used to generate the required isotherms is given in the Appendix.

As mentioned previously, experiments have been performed at high pressures with metal foams and loosely packed powders. The data from these experiments are limited to small distentions and can be described by either the plate-gap model or the Russian equation of state. The program described here was intended to provide experimental shock compression data for porous copper at high distentions up to about 0.9 Mb. The results of these experiments would then be compared to the predictions of the available theories.

SECTION II

DESCRIPTION OF EXPERIMENTS

EXPERIMENTAL CONSIDERATIONS

For this study an "accelerated reservoir" light-gas gun was used to launch flyer plates at velocities nearing 8 kilometers per second. The light-gas gun range and basic instrumentation have been described in several other papers[7-10]. This method of experimentation offers significant advantages over the explosive techniques previously used. Unshocked, stress-free impactors of dissimilar material to the specimen can be impacted over a wide and continuous velocity range.

By varying the impact velocity and the impactor impedance and measuring the shock propagation parameters of the target a shock adiabat may be determined. This simple approach has been employed to establish the high pressure Hugonicts for a number of materials as in Reference 8. These shock wave parameters are the shock velocity and the mass velocity or particle velocity behind the shock front. In addition to these two values, several assumptions are implied in the Rankine-Hugoniot equations used to describe the effect on the material of the shock wave. The equations are:

$$P_H - P_o = \rho_o U_s u_p \tag{21}$$

$$V/V_o = 1 - u_p/U_s \tag{22}$$

$$E_H - E_o = 1/2\ (P_H - P_o)\ \ (V_o - V) \tag{23}$$

where the subscripts o and H refer to the conditions in front of and behind the shock front respectively and

P is pressure

$\rho = 1/V$ or density

V is specific volume

U_s is shock velocity

u_p is particle velocity

E is specific internal energy

These equations assume a discontinuity in P, ρ and E across the shock front and that P_H, ρ_H and E_H represent thermodynamic equilibrium conditions.

The two standard techniques employed by our laboratory both involve accurate and precise measurements of the impactor velocity.[8] Technique I is used when the target and impactor material are identical. In this case $u_p = 1/2\ v_i$, v_i = impact velocity. We have previously established that the impactor after launch but prior to target impact is essentially unshocked and thermodynamically at the initial state. Technique II is used for dissimilar material impacts and depends upon detailed knowledge of the Hugoniot equation of state of the impactor material. The process of establishing the Hugoniot standards for these experiments is Technique I. Even though any given Hugoniot state of a standard is precise to $\sim$ 0.5%, because of the statistical nature of the descriptive

equation (usually a linear least squares data fit) the resulting U_s (u_p) equation is only accurate to about 2%. The use, then, of Technique II usually results in Hugoniot data in the unknown material of an accuracy of ∿ 2-4%. The assumption of instantaneous state discontinuity (ignoring low pressure elastic waves) ensures that the high pressure shock process is truly adiabatic, i.e., all the change in internal energy occurs from compression alone, and, without extremely difficult stepwise analysis, is the only way to describe the shock on a macroscopic scale. In addition, the assumption of thermodynamic equilibrium establishes the only basis at present for analytical treatment of the shock data from endpoint to endpoint. If either of these assumptions fail at high pressures, the Hugoniot interpretation of the measurements also fails. There are several possible ways this might be observed.

a. Nonsteady shock propagation. Since it is obvious that shock waves do attenuate the criterion must be established at some limit. Primarily very high pressure shocks attenuate geometrically, but many materials evidence irreversible energy losses through phase transitions both solid/solid type and solid/liquid or solid/liquid/gas. This is observable by non-constant shock propagation velocities with increasing specimen thickness.

b. Cross correlation of state measurements. Shocks might exhibit non-equilibrium conditions if the experimental redundancy of recording systems are accurate enough. An example might be the simultaneous measurement of the shock

pressure-time history and shock velocity, or some other shock parameter which would allow redundant calculation of the shock state.

c. The appearance of structured or multiple waves. Multiple waves at very high pressures may indicate the existence of non-equilibrium conditions behind the shock, assuming that phase transitions are accounted for.

MATERIAL DESCRIPTION

The distended copper employed as test material was produced by a process developed at GM Research, General Motors Technical Center, Warren, Michigan. Known as MetNet, the specimens bulk properties are shown in Table I. Microscopic examination reveals that the copper MetNet structure is weblike. The webbing is the interstitial volume between tightly packed spheres of nearly identical diameter as shown in Figure 1.

Each cell interconnects with its neighbors through nearly circular openings - the number of openings depending on the diameters of the cell and its neighbors. Openings per cell range from 10 to 15. The cross section of the intracellular web is triangular with the three sides concave outward, and a similar triangular hollow center. The geometry remains identical with increasing density only the cross sectional thickness of web increases.

The target densities of approximately 33%, 22% and 11% of solid copper were selected as compromises between the constraints of

TABLE I

PHYSICAL PROPERTIES OF COPPER METNET

Sample Average Density			
(gm/cm^3):	2.94	1.99	1.001
Distention:	3.08 rms 0.03	4.46 rms 0.03	8.74 rms 0.08
Spectro/Chemical Analysis*			
Element % Comp.			
Copper	99.02	98.30	96.99
Nickel	0.92	1.49	2.38
Zinc	Trace	Trace	0.43
Iron	Trace	0.10	Trace
Pore Size			
Range (in.):	0.008"- 0.035"	0.010"- 0.040"	0.010"- 0.040"
Approx. Ave. (in.)	0.012"	0.015"	0.015"
Sound Speed			
Approx. Longitudinal Vel. (mm/μsec)	1.92	1.55	0.98

* Tests performed by Met-Chem Testing Laboratories, Inc. 20062 John R, Detroit, Michigan.

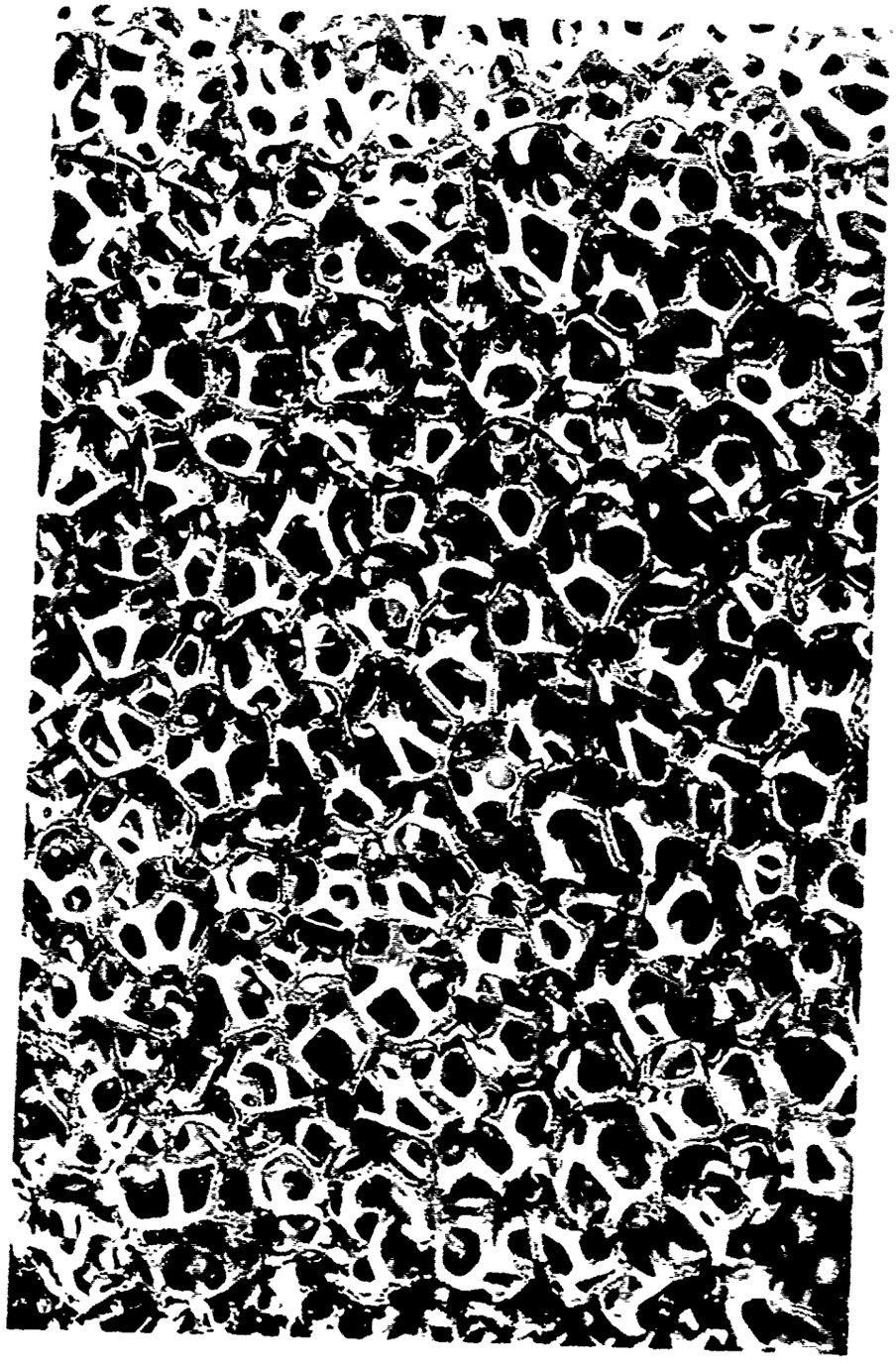

Figure 1 Photomicrograph of Copper MetNet

the manufacturing process - i.e. limited maximum densities of ∿ 50% solid, and mechanical requirements for handling. MetNet can be produced at distentions of 100 or more.

The specimen densities and porosities were determined by two methods: a) water saturated, dry and immersed weights and b) bulk dimensions with dry weights.

All target and test specimens were taken from single 10" x 12" sheets 1/4" thick for each distention. Density measurements were made on each target specimen as well as on several selected samples from locations throughout the respective sheets. The water immersion method was employed and by soaking the specimens overnight in a pressurized water bath, the bulk density and porosity measurements were within 0.5% of the values determined geometrically. Individual bulk density measurements may tend to be in error due to the small sizes for some of the target specimens, nevertheless, the measured values shown in Table II, III, and IV are employed in the Hugoniot calculations.

The nickel contaminant shown in Table I is a result of the manufacturing process for MetNet but is sufficiently low in view of the great distentions to not be a significant factor in the high pressure behavior.

SPECIMEN PREPARATION

Target specimens were core drilled from the stock sheets slightly oversize. Turning to final test diameter was performed after one face of the target was machined flat. It was learned that although the machining operations tended to

smear and distort the web network, the deformed zones could be removed by lapping since they were only about three pore diameters thick. The lapped surfaces appeared microscopically to be nearly ideal cross sections of the foam. For the most part, the target edges were left in the smeared condition since this enhanced target mounting by epoxy casting. Care was taken to seal the specimen edges so that the mounting epoxy did not seep into the target thus changing its apparent bulk density.

The planarity of the lapped target faces was checked on a Zeiss light section microscope. While the surface roughness was of the order of the cellular diameters, the sectioned webbing was uniform and the impact and rear surfaces coplanar to within $\sim$ 0.0001 inch.

Oxidation and corrosion of the copper was kept to a minimum by storing the specimens in a vacuum desiccator after they were annealed in a reducing atmosphere.

Target handling was a problem only for the highest distention MetNet which could be deformed by finger tip pressure. Mounting and machining fixtures and careful handling prevented inadvertant marring collapsing of the test specimens.

TARGET DESIGN

Pin Targets

The majority of the targets used in these experiments were of the four pin design described in earlier papers[7,8]. The instrumentation of these targets permitted the measurement of

two shock transit time intervals during each shot, as well as a recording of the impactor tilt relative to the pin axis.

Several 5 cm diameter targets were instrumented with mica sheathed manganin wire piezoresistive transducers[11]. Front and rear surface pins were also used to measure the shock transit time. These targets consisted of two disks ∿ 4.5 mm thick with the sheathed gage sandwiched in between. Although several versions of sheathing and assembly were constructed, none of them successfully recorded a pressure profile.

Optical Targets

Several targets were designed to be optically instrumented by a Beckman and Whitely Model 339B high speed continuous-writing streak camera. Three wedge shaped targets were tested at the three distentions for nonuniform shock propagation with thickness at relatively low pressure. Target design is shown in Figure 2. Light reflecting from the front surface mirror/target interface is extinguished upon the arrival of a shock, thus photographically permitting continuous shock transit time interval determination. A record obtained from these shots is shown in Figure 3 and graphical reductions of Shots 401, 407 and 408 are shown in Figures 4, 5, 6 and 7.

Single and double step targets were constructed for use at higher impact velocities than the three shots above. The design for these targets is shown in Figure 8. Over the range of impact velocities achievable by the 29 mm launch tube all the impact events are self-luminous, i.e., the impactor strike at the target front surface, and the arrival of the shock at the rear surface glass witness plate are light emitting events. Figure 9 displays one such experiment record.

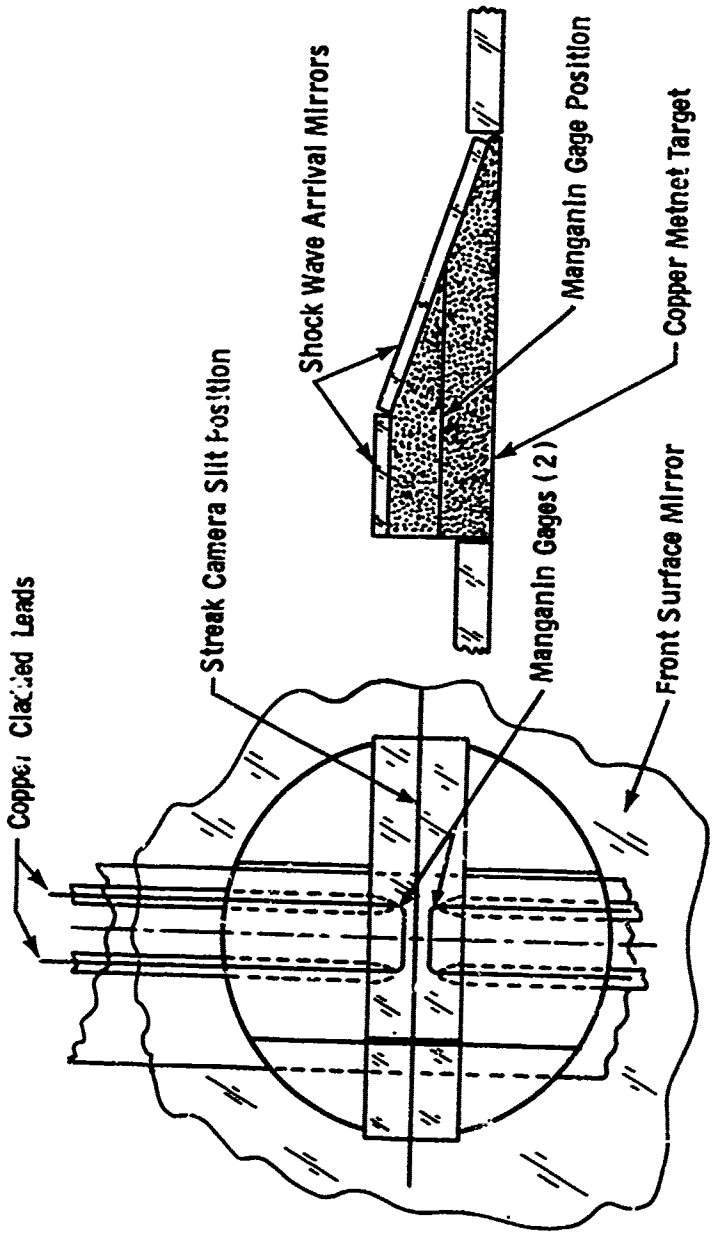

Figure 2 Design of Optical Wedge and Manganin Gage Target

Figure 3 Streak Camera Record of an Optical Wedge Experiment

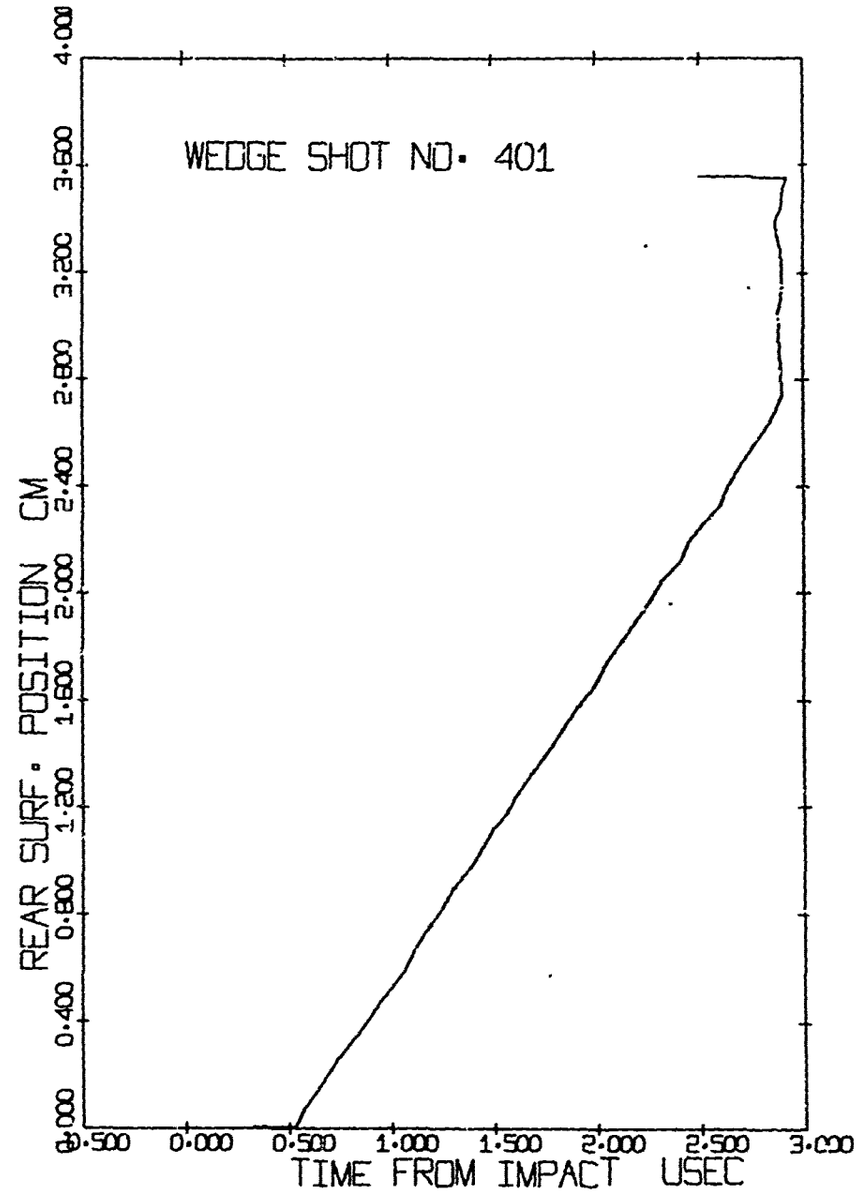

Figure 4 Computer Plot of Position of Shock Wave on Wedge from Time of Impact

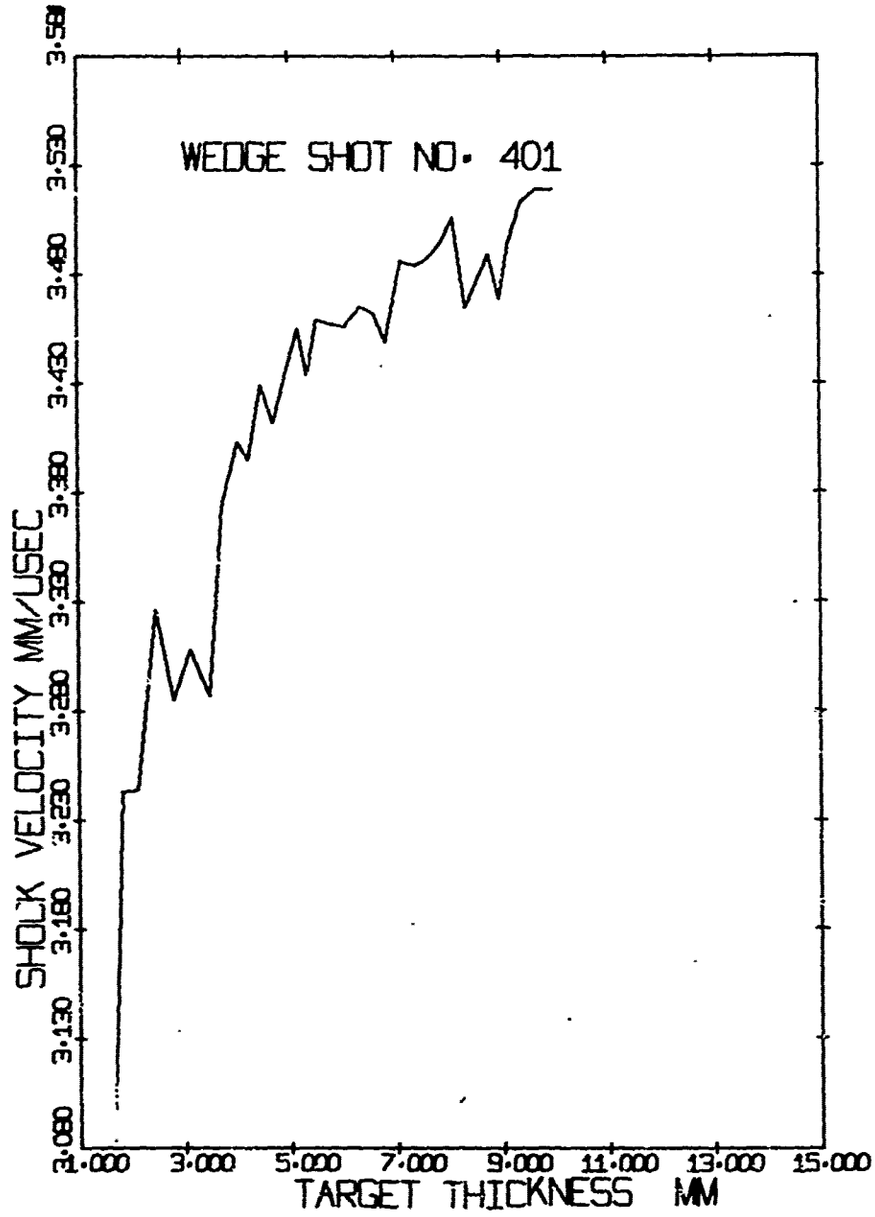

Figure 5 Optical Wedge Target, Shock Velocity vs. Target Thickness, Shot No. 401

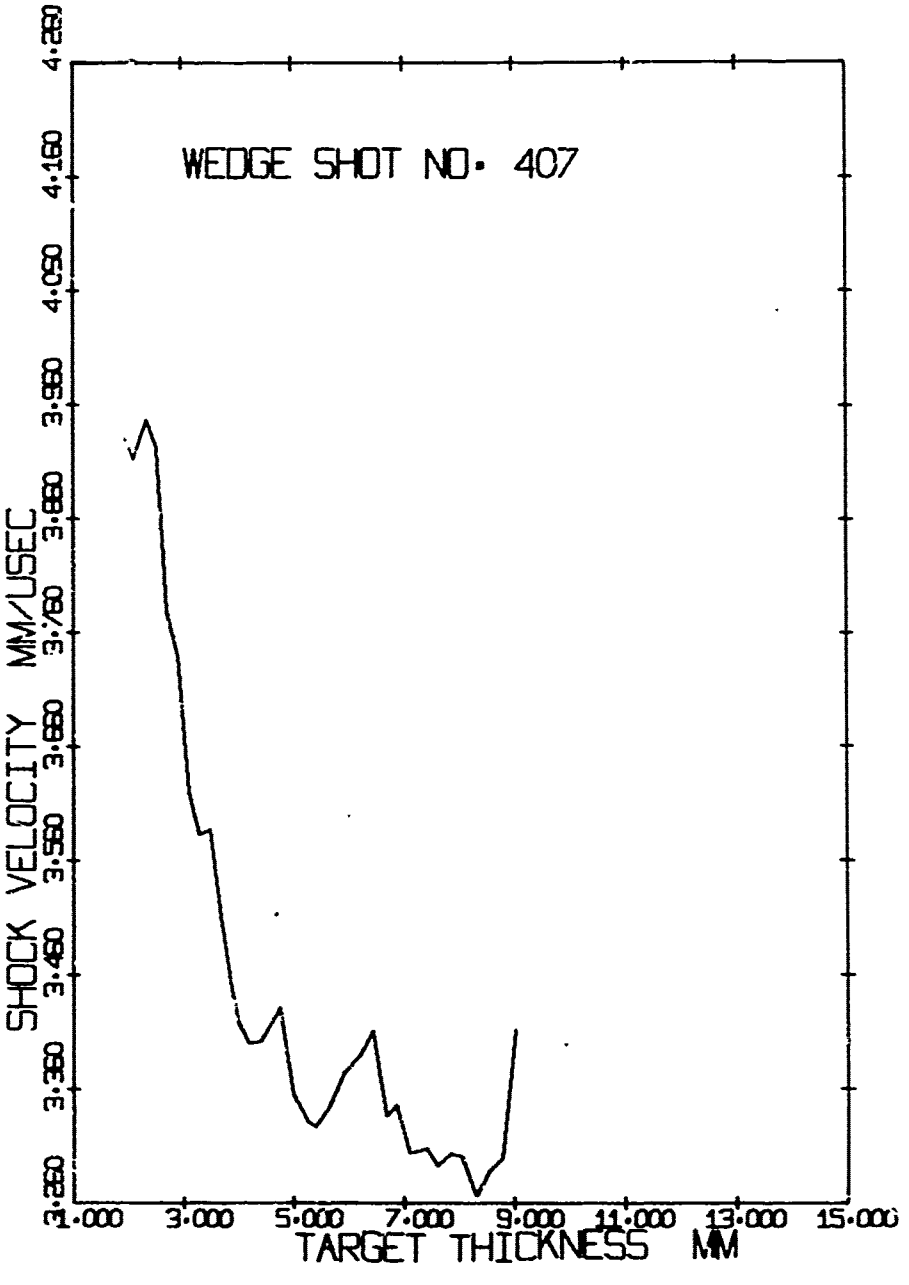

Figure 6 Optical Wedge Target, Shock Velocity vs. Target Thickness, Shot No. 407

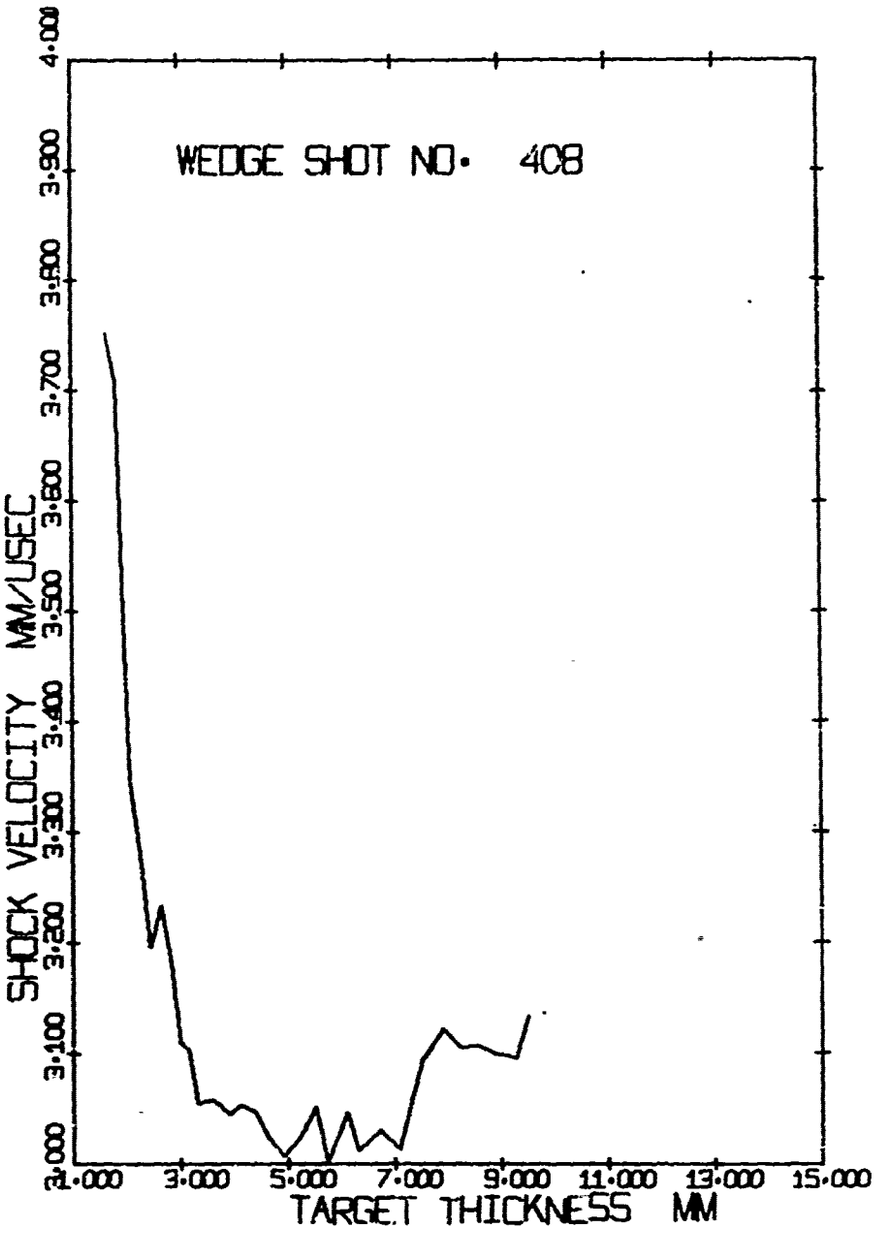

Figure 7 Optical Wedge Target, Shock Velocity vs. Target Thickness, Shot No. 408

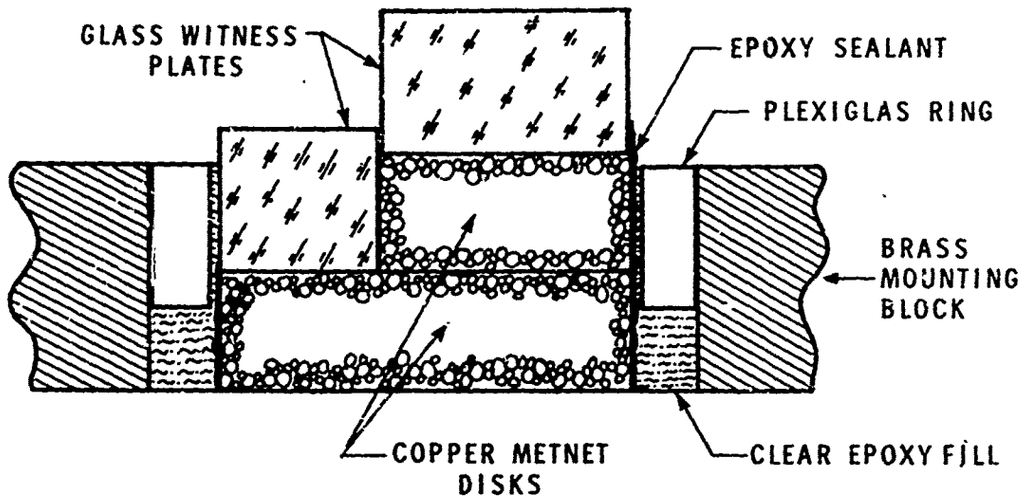

Figure 8 Design of Optical Double Stepped Target for High Pressure Experiments

Figure 9 Streak Camera Record of Double Step Target High Velocity Impact

A single optical test was performed which was also instrumented by pins. This shot was designed to cross check the correlation with the pin-only target data to the optics-only target results.

DATA ANALYSIS

The basic parameters measured in these experiments were the impact velocity of the impactor and shock velocity.

The impactor velocity measuring system consists of a laser triggering system and two short duration flash X-rays.[8] With this system, impactor velocities are measured accurately to 0.05%. The triggering system consists of a helium-neon gas laser aimed at a photo-detector across the impact chamber, orthogonal to and intersecting the line of flight of the projectile. A photomultiplier monitors the laser light output through a set of masks and a narrow bandpass optical filter. When light interruption occurs due to projectile passage, a sharp change of voltage level is converted into a signal of sufficient amplitude to trigger a Field Emission Corporation 30 nanosecond dual flash X-ray unit. The X-ray flash exposes a Polaroid film plate on the opposite side of the chamber by means of a fluorescing intensifier screen. The trigger and X-ray flash system is then duplicated to record the passage of the projectile in the second field of view 30.5 cm further down range.

The spacing between the two X-ray field centerlines is indicated by fiducial wires which are measured by an optical comparator to within 0.2 mm. Measurements of the impactor face position relative to the window fiducials allow calculation

of actual projectile position and travel over the time interval measured between flash exposures.

Measurement of shock velocities was accomplished through recording of the time interval between impact and shock arrival. The closure of coaxial self-shorting pins provided signals to start and stop Eldorado Model 793 time interval meters. These counters have a specified time resolution of $\pm$ 1/2 nsec and are read digitally to the nearest nsec.

The optical records were converted to time intervals through reduction from analog to digital form using an optical comparitor. The digital records are then computer analyzed into time intervals and shock wave velocities. Corrections for impactor tilt, target surface non-parallelism, and statistical averaging are employed in the computer analysis. The actual measurements are relative time positions on stationary film in the continuous writing streak camera. These relative film event positions are converted to time intervals in terms of the camera writing rate through knowledge of the turbine angular velocity and corrections are applied for the optical and mechanical nonlinearities.

Although all the data here are presented as shock velocities, it should be kept in mind that the actual recorded data is in the form of relative event times and velocities are inferred on the assumption of constant velocities.

SECTION III

EXPERIMENTAL RESULTS

This section presents the results of the data analysis previously described. A few preliminary remarks are necessary. The attempts to record the pressure-time profiles of the three distentions of MetNet were unsuccessful. All of the sheathed manganin wire transducers imbedded in the targets shorted immediately upon the arrival of the transmitted wave. We have no experimental evidence enabling us to ascertain whether the shorting occurred along the gage leads or in the active area. Even additional buffering by increasing the sheath thickness had no apparent effect on gage lifetime. Interpretation of the three wedge targets at the relatively low impact velocity of $\sim$ 2.85 km/sec was that no appreciable wave propagation velocity change occurs in the thickness range from 2 to 10 mm. Thus, a single thickness of $\sim$ 5 mm was employed for most of the pin experiments.

PIN DATA

Compilations of the pin experimental results are presented in Tables II, III and IV for copper MetNet at the average distentions of m_{ave} = 3.08, 4.46 and 8.74 respectively. These data are displayed simultaneously in the shock velocity-particle velocity plot, Figure 10. Simple curves drawn through the data suggests that experimental scatter is quite significant. Interpreting the scatter as curvative is rather dubious since

TABLE II

PIN DATA FOR DISTENDED COPPER, m_{ave} = 3.08

SHOT	DISTENTION ρ_o/ρ_{oo}	SHOCK VEL. km/sec	PARTICLE VEL. km/sec	PRESSURE Megabar	SPECIFIC VOL. cc/gm	IMPACT VEL. km/sec	IMPACTOR MATERIAL
437	3.18	4.26				3.984	OFHC Cu
439	3.09	4.901	3.075	0.435	0.1290	3.994	OFHC Cu
	3.09	4.872	3.079	0.433	0.1274	3.994	OFHC Cu
434	2.94	6.955	4.076	0.860	0.1364	5.6223	OFHC Cu
	2.94	6.690	4.110	0.835	0.1271	5.623	OFHC Cu
430	3.10	8.149	5.217	1.226	0.1247	6.498	OFHC Cu
	3.10	8.019	5.230	1.210	0.1206	6.498	OFHC Cu
453	2.98	9.325	5.96 ± .12	1.664 ± .035	0.121 ± .005	7.57 ± .15	FS-77*
449	2.91	9.515	6.047	1.768	0.1186	7.738	FS-77*
525	3.097	6.51	4.16	.78	.125	5.60	OFHC Cu
		6.19	4.20	.75	.111	5.60	
527	3.107	8.63	5.41	1.34	0.130	6.785	FS-77*
		8.30	5.46	1.30	0.120	6.785	

* FS-77 = Fansteel-77

TABLE III

PIN DATA FOR DISTENDED COPPER $m_{\bar{a}ve} = 4.46$

SHOT	DISTENTION ρ_o/ρ_{oo}	SHOCK VEL. km/sec	PARTICLE VEL. km/sec	PRESSURE Megabar	SPECIFIC VOL. cc/gm	IMPACT VEL. km/sec	IMPACTOR MATERIAL
419	4.34	3.512	2.675	0.194	0.1156	3.1420	OFHC Cu
	4.34	3.583	2.668	0.197	0.1239	3.1420	OFHC Cu
436	4.58	4.720	3.257	0.330	0.1444	3.9901	OFHC Cu
	4.58	4.693	3.259	0.328	0.1423	3.9901	OFHC Cu
433	4.53	6.434	4.447	0.565	0.1565	5.5734	OFHC Cu
	4.53	6.577	4.431	0.575	0.1654	5.5734	OFHC Cu
429	4.47	8.017	5.437	0.918	0.1529	6.4547	FS-77*
	4.47	7.917	5.446	0.907	0.1483	6.4547	FS-77*
452	(3.80)*	9.128	6.249 ± .043	1.341 ± .009	0.1343 ± .0021	7.6204	FS-77*
450	(3.87)*	9.870	6.32 ± .13	1.439 ± .030	0.156 ± .006	7.77 ± .13	FS-77*

* FS-77 Fanstael-77

( ) Sample measurement may be in error

TABLE IV

PIN DATA FOR DISTENDED COPPER, m_{ave} = 8.74

SHOT	DISTENTION ρ_o/ρ_{oo}	SHOCK VEL. km/sec	PARTICLE VEL. km/sec	PRESSURE Megabar	SPECIFIC VOL. cc/gm	IMPACT VEL. km/sec	IMPACTOR MATERIAL
418	8.91	3.631	2.912	0.104	0.2007	3.1804	OFHC Cu
	9.06	3.684	2.909	0.106	0.2134	3.1804	OFHC Cu
435	8.59	4.571	3.560	0.169	0.2127	3.9744	OFHC Cu
	8.59	4.555	3.561	0.169	0.2099	3.9744	OFHC Cu
432	8.43	6.482	4.798	0.330	0.2450	5.5313	OFHC Cu
	8.43	6.602	4.788	0.335	0.2592	5.5313	OFHC Cu
428	8.45	7.775	5.886	0.484	0.2299	6.4824	OFHC Cu
	8.45	7.584	5.897	0.473	0.2104	6.4824	OFHC Cu
456	8.47	9.424	6.656	0.661	0.2790	7.4347	FS-77*
451	8.71	10.145	6.979	0.726	0.3044	7.8202	FS-77*

* FS-77 - Fansteel-77

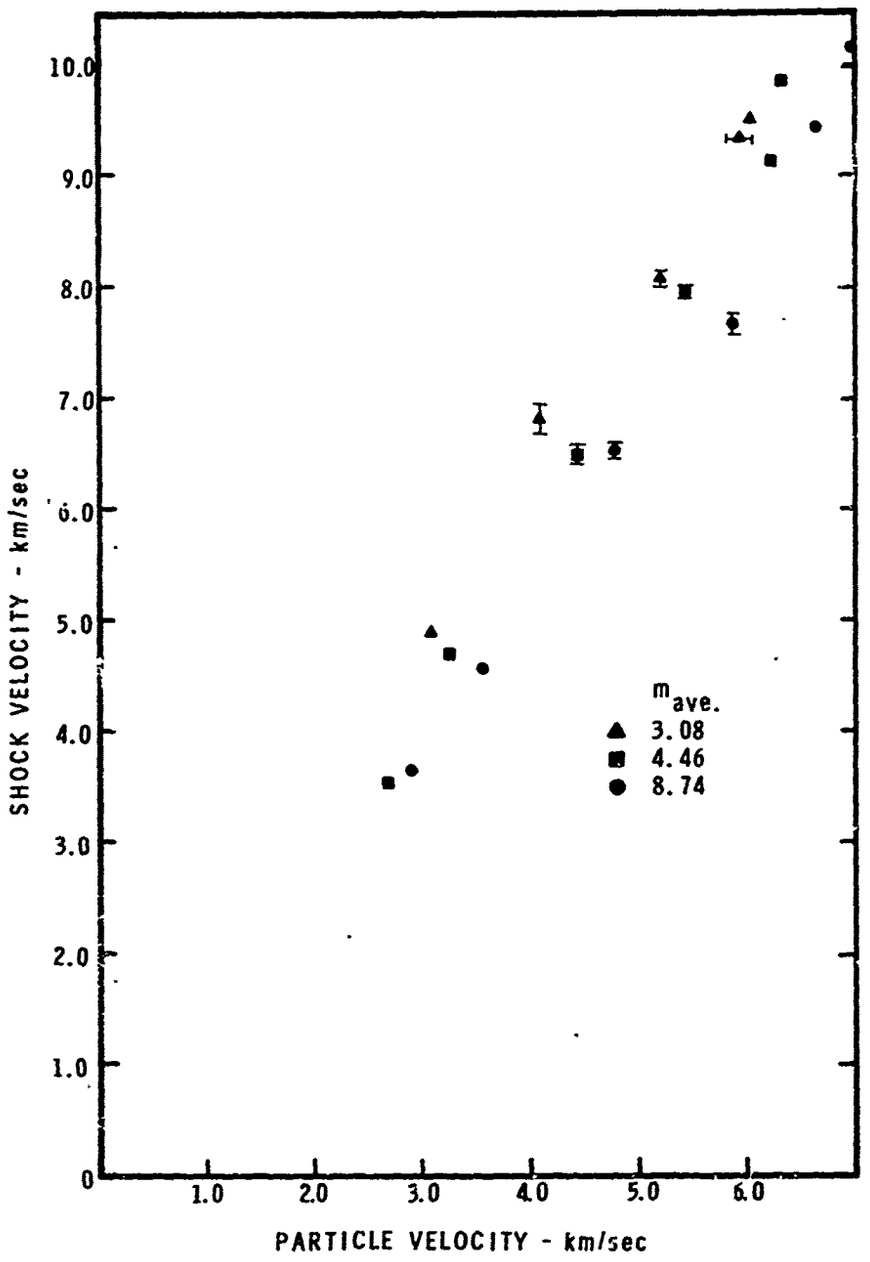

Figure 10 Pin Data for Distended Copper, Shock Velocity vs. Particle Velocity

conversion to the pressure-volume plane results in double and possibly triple valued states at some values of V. This may be seen in Figure 15 by simply connecting the dots.

OPTICAL DATA

Tables V, VI and VII present the numerical results from the optical records as well as all the pin data. A different interpretation had to be made of these records than for the pin records. The recording time of these optical experiments was much longer than with the pin technique. That is, optical recording of events is possible as long as the glass witness plate remains undestroyed. These glass witness plates were not silvered so that events prior to the actual rear surface arrival were observable. Figure 11 is a record of Shot 521 into a target with no step and $\sim$ 9 mm thick, showing, 1) the arrival at the target front face, 2) luminousity from inside the open celled structure, 3) arrival at the witness plate of the luminous streams, 4) arrival at the interface of a destructive wave, and 5) arrival of that destructive wave at the rear surface of the witness plate.

Events 3 and 4 are characterized more as zones of changing luminousity. An indication of the substantial energy represented by the discrete luminous streams is the shock diamond pattern in the glass witness plate just after Event 4. The time interval of Event 4 is identifiable in all the optical records and is significantly larger than that recorded by the self-shorting pins. In fact, the pin recorded time intervals for nearly identical impact conditions (and for Shot 527 identical impact conditions) corresponds to the optical Event 3. In addition, the scatter in the pin records correlates well with

TABLE V

OPTICAL AND PIN DATA FOR DISTENDED COPPER, m_{ave} = 3.08

Shot	Minimum No. Of Cells	v_i (km/sec)	$\frac{\rho_o}{\rho_{oo}}$	ρ_{oo} (gm/cm^3)	OPTICAL DATA		PIN DATA		TARGET THICKNESS	
					Last Wave v_s (km/sec)	First Wave U'_R (km/sec)	Pin Sta A U'_{sa} (km/sec)	Pin Sta B U'_{sb} (km/sec)	H (mm)	Average Δt (μsec)
526	15	2.768	3.077	2.876			3.38		4.74	
	30			2.928				2.70	9.51	
401	33	2.913	3.042	2.936	2.78	3.30			10.11	0.58
529	15	3.928	3.067	2.807	4.81	5.14			4.51	0.06
	30			3.016	4.03	4.14			9.13	0.06
437	16	3.984	3.181	2.807			4.26		5.01	
439	16	3.994	3.092	2.889			4.90	4.87	5.02	
525	15	5.60	3.097	2.777			6.51		4.70	
	30			2.990				6.19	9.45	
434	15	5.623	2.942	3.035			6.69	6.96	4.68	
528	15	5.689	3.113	2.851	5.97	6.47			4.69	0.06
	30			2.886	5.89	6.16			9.54	0.07
430	16	6.498	3.096	2.885			8.15	8.02	5.01	
521	30	(7.332)	3.301	2.705	7.60	8.10			9.25	0.06
527	15	(7.510)	3.107	2.874	7.90	8.73	8.63	8.30	4.76	0.05
453	16	(8.420)	2.981	2.996			9.33		5.07	
449	16	(8.614)	2.905	3.074			9.52		5.06	

TABLE VI

OPTICAL AND PIN DATA FOR DISTENDED COPPER, $m_{ave} = 4.46$

Shot	Minimum No. Of Cells	v_i (km/sec)	$\frac{\rho_o}{\rho_{oo}}$	ρ_{oo} (gm/cm^3)	OPTICAL DATA		PIN DATA		TARGET THICKNESS	
					Last Wave U_s (km/sec)	First Wave U'_s (km/sec)	Pin Sta A U'_{sa} (km/sec)	Pin Sta B U'_{sb} (km/sec)	H (mm)	Average Δt (μsec)
---	---	---	---	---	---	---	---	---	---	---
407	24	2.852	4.487	1.990	2.65	3.29			9.35	0.28
419	12	3.142	4.333	2.061			3.51	3.58	4.83	
	24			2.058					10.17	
436	12	3.990	4.575	2.147			4.69	4.72	4.99	
433	12	5.573	4.526	1.973			6.58	6.43	4.09	
530	11	5.737	4.466	2.058	5.77	6.48			4.53	0.07
	22			1.941	5.79	6.35			8.46	0.07
531	11	6.091	4.518	1.977	7.48	8.30			4.27	0.08
	22			1.977	7.69	8.04			8.59	0.05
429	13	(7.058)	4.465	2.105			7.92	8.02	5.00	
452	13	(8.371)	3.800	2.350			9.13		5.05	
459	13	(8.552)	3.871	2.306			9.87		5.06	

TABLE VII

OPTICAL AND PIN DATA FOR DISTENDED COPPER, m_{ave} = 8.74

Shot	Minimum No. Of Cells	v_i (km/sec)	$m \cdot \frac{\rho_o}{\rho_{oo}}$	ρ_{oo} (gm/cm^3)	OPTICAL DATA: Last Wave U_s (km/sec)	OPTICAL DATA: First Wave U'_s (km/sec)	PIN DATA: Pin Sta A U'_{sa} (km/sec)	PIN DATA: Pin Sta B U'_{sb} (km/sec)	TARGET THICKNESS H (mm)	Average Δt (μsec)
408	25	2.869	8.921	1.001	2.63	3.11			9.84	0.57
418	12	3.180	8.984	1.002			3.63		4.84	
	25			.995				3.60	9.84	
435	13	3.974	8.591	1.040			4.56	4.57	5.01	
432	13	5.531	8.429	1.060			6.60	6.48	5.00	
532	10	5.757	9.131	1.008	5.71	6.78			3.82	0.11
	20			0.948	5.60	6.41			7.83	0.10
428	13	(6.884)	8.451	1.057			7.58	7.78	5.00	
522	20	(7.068)	8.704	1.026	7.05	7.67			7.93	0.06
456	13	(7.928)	8.473	1.054			9.43		5.06	
451	13	(8.380)	8.712	1.025			10.15		5.06	

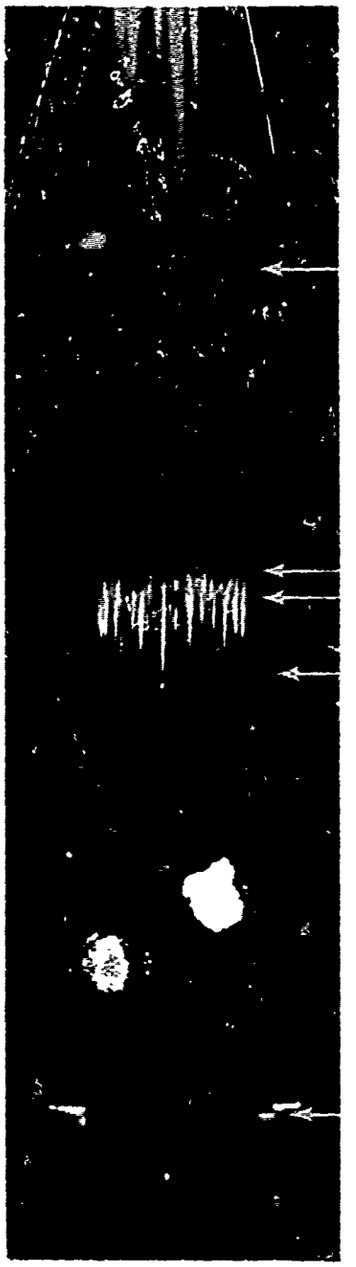

Figure 11 Single Step Optical Target Impact Events

the optically observed irregularity of stream arrivals. Tables V, VI, and VII are also compilations of all the experimental work at the three MetNet distentions. The shock wave velocity data are correlated to copper impactor velocity and segregated by recording technique and recording station position. The impact velocities contained in parentheses are computed values, i.e. the velocity a copper impactor would have to induce the same state in the target that was achieved by the actual Fansteel-77 impact. The optical data columns contain the recorded velocities of both the first and the final "waves", and in the cases of the stepped targets both thickness station values are listed separately but under the same shot number. The approximate time interval between the two waves is listed in column "Average Δt." The pin data are tabulated under either station A or B and the station thicknesses are listed.

Figures 12, 13 and 14 are shock velocity-impact velocity plots of the data contained in Tables V, VI, and VII respectively. Shot numbers are included to identify the impact velocities for the experiments. The endpoints of the error bars show the first and last wave velocities for the optical shots and the data scatter for the pin shots.

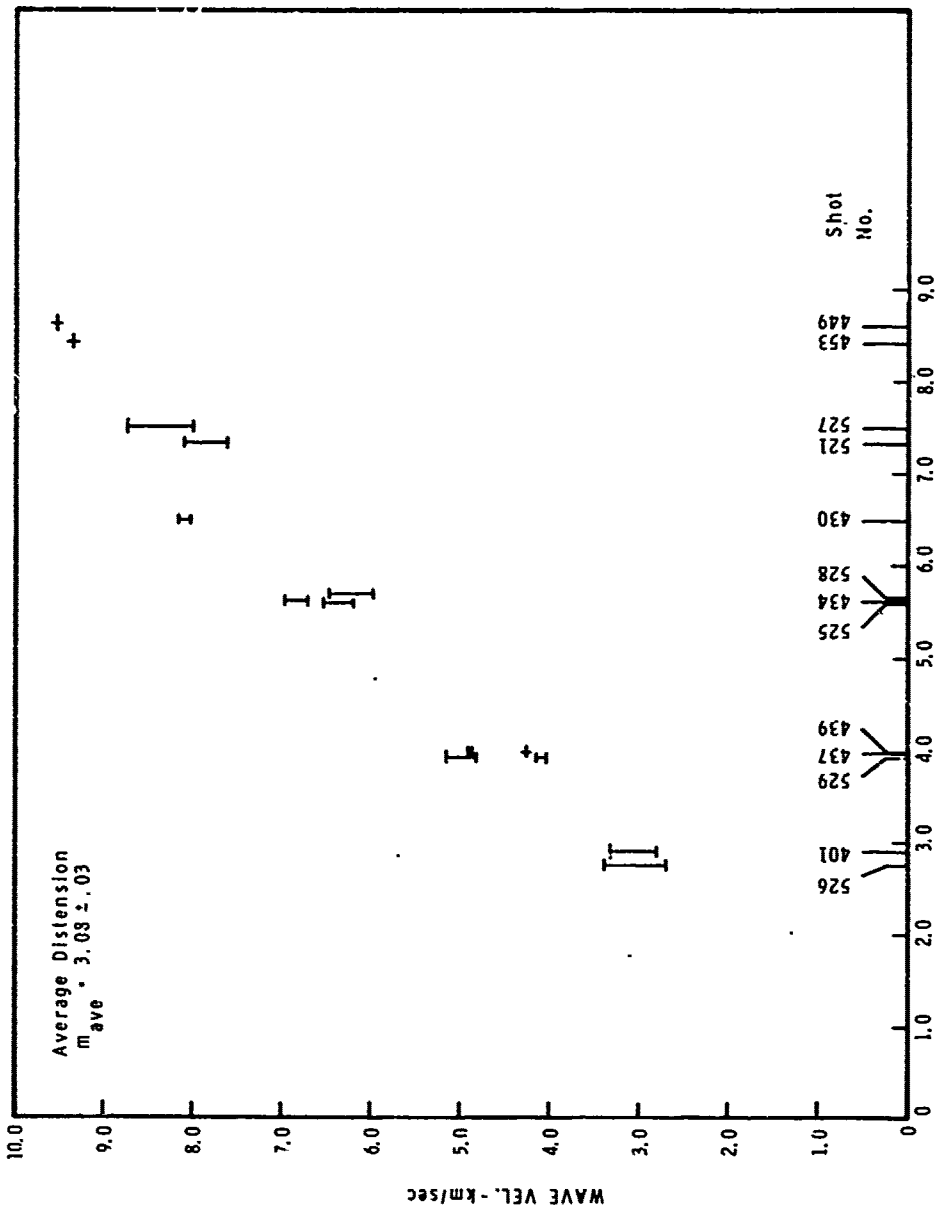

Figure 12 Wave Velocity vs. Impact Velocity for m_{ave} = 3.08

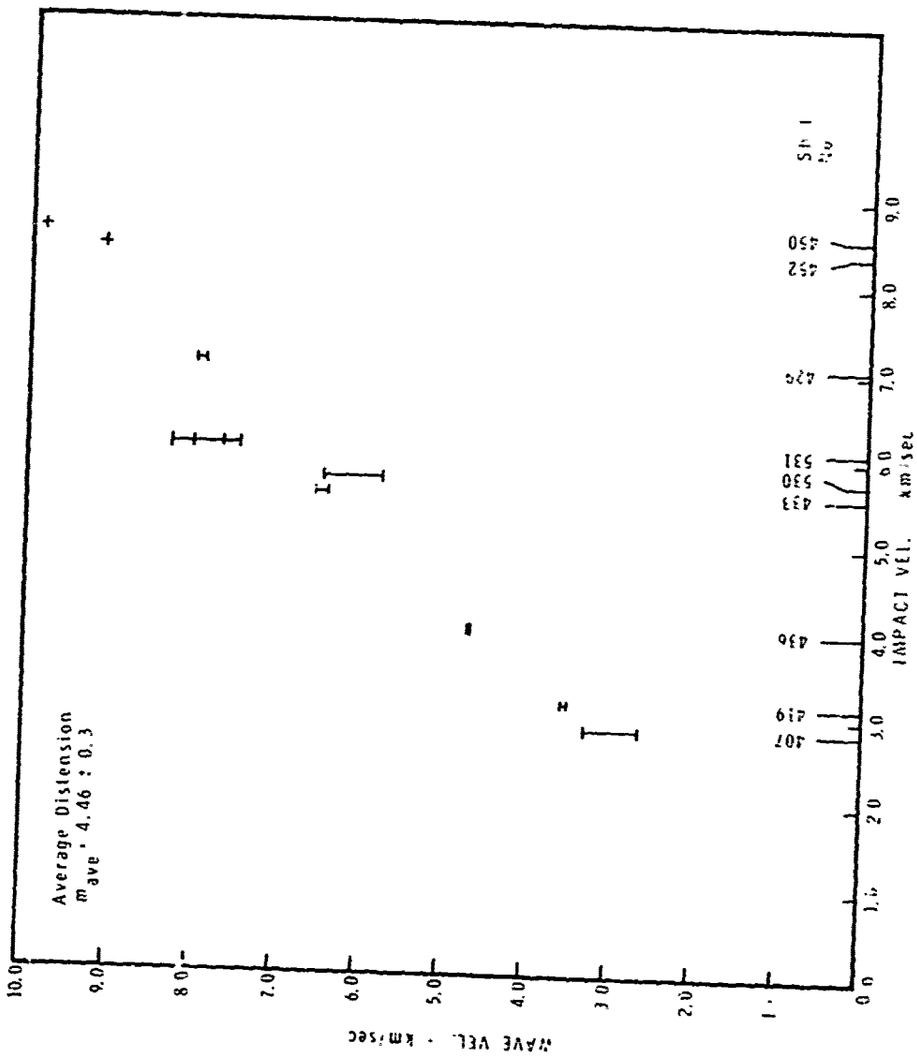

Figure 13 Wave Velocity vs. Impact Velocity for m_{ave} 4.46

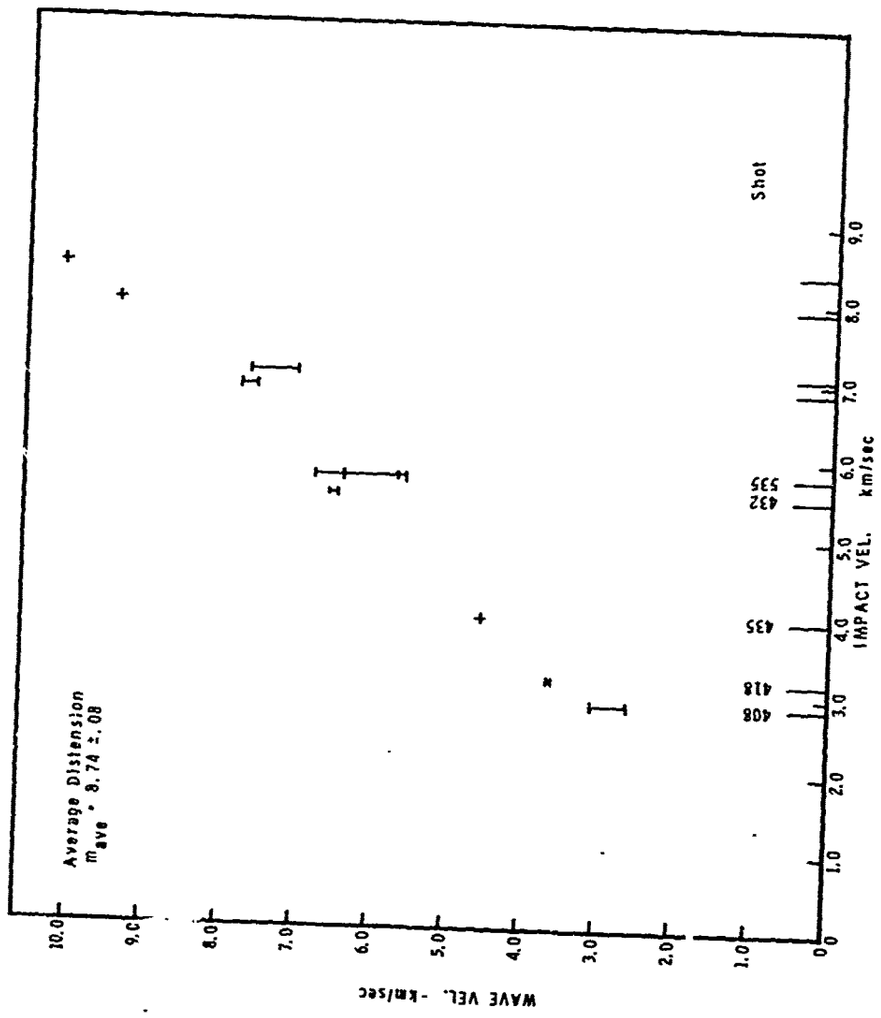

Figure 14 Wave Velocity vs. Impact Velocity for m_{ave} = 8.74

SECTION IV

DISCUSSION OF RESULTS

COMPARISON OF PIN DATA TO RUSSIAN WORK

A primary objective of the program described here was to compare experimentally similar materials testing between our efforts at large distentions and the Russian Work[1,2] with distended copper at m = 1.57, 2.0, 3.01 and 4.0. Our distentions were m = 3.08, 4.46 and 8.74. The experiments at m = 3.01 and 3.08 were expected to overlap. Since essentially identical experimental techniques were employed (except for impactor velocities), i.e. electronic pin switches, similar target size, time interval measuring, any significant differences in results can only be attributable to the specimen structure itself. As can be seen in Figures 15 and 16, there is considerable difference between the pin recorded states of this and the Russian work. Dashed lines are used to indicate the predicted Hugoniots for the values of m shown. The pin data plotted for these distentions also deviate significantly from the predicted Hugoniots. The Russian experimental data are plotted with open symbols as shown in the legend.

QUALITATIVE DISCUSSION OF OPTICAL RECORDS

The additional observations performed by us, i.e. the optical tests, suggest a mechanism for the above discrepancies. From the fact that our records show a displacement in the P-V plane to the right of the predicted Hugoniots it can be inferred that our recorded shock velocities are too high. Indeed, the optical

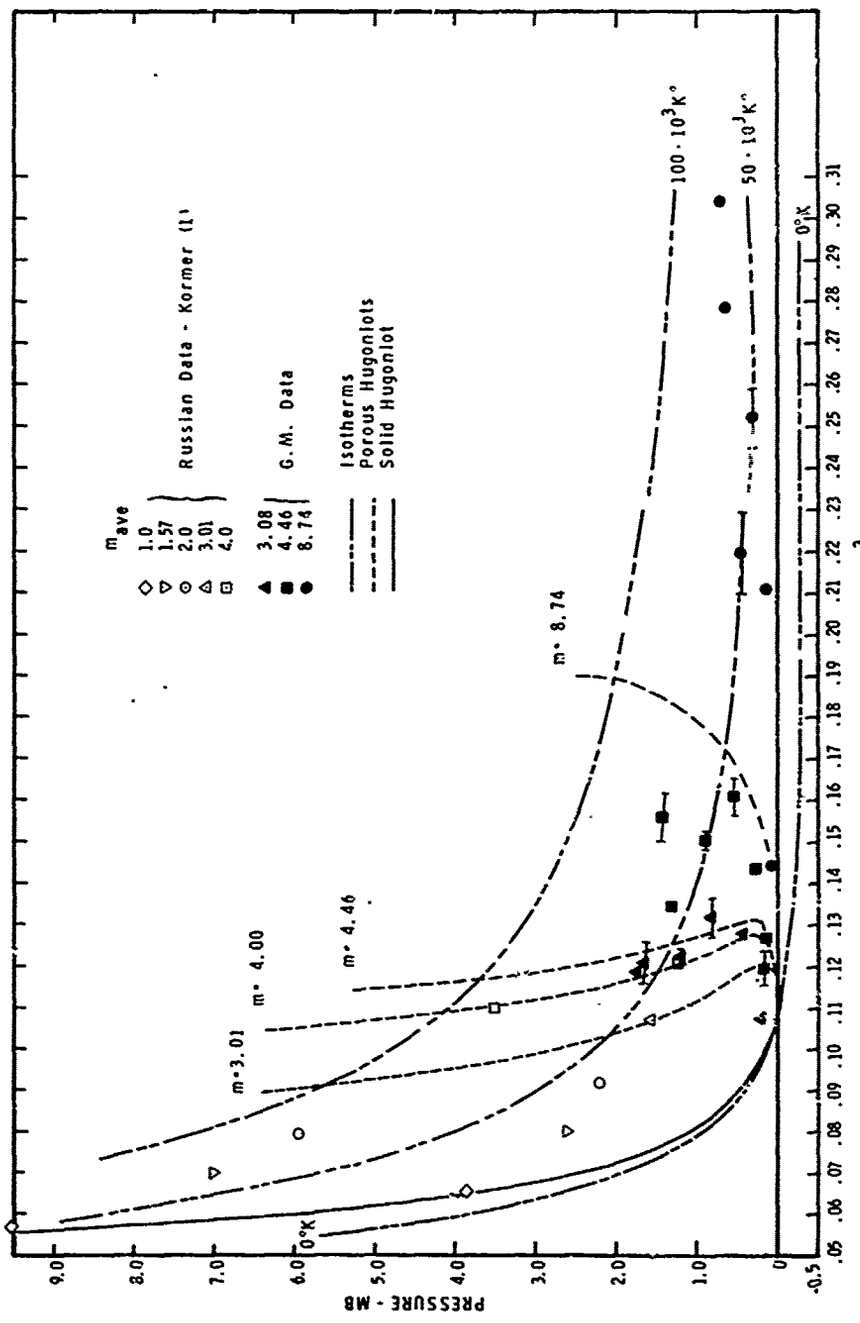

Figure 15 Pressure - Volume Diagram of Copper: Comparison with Russian Data

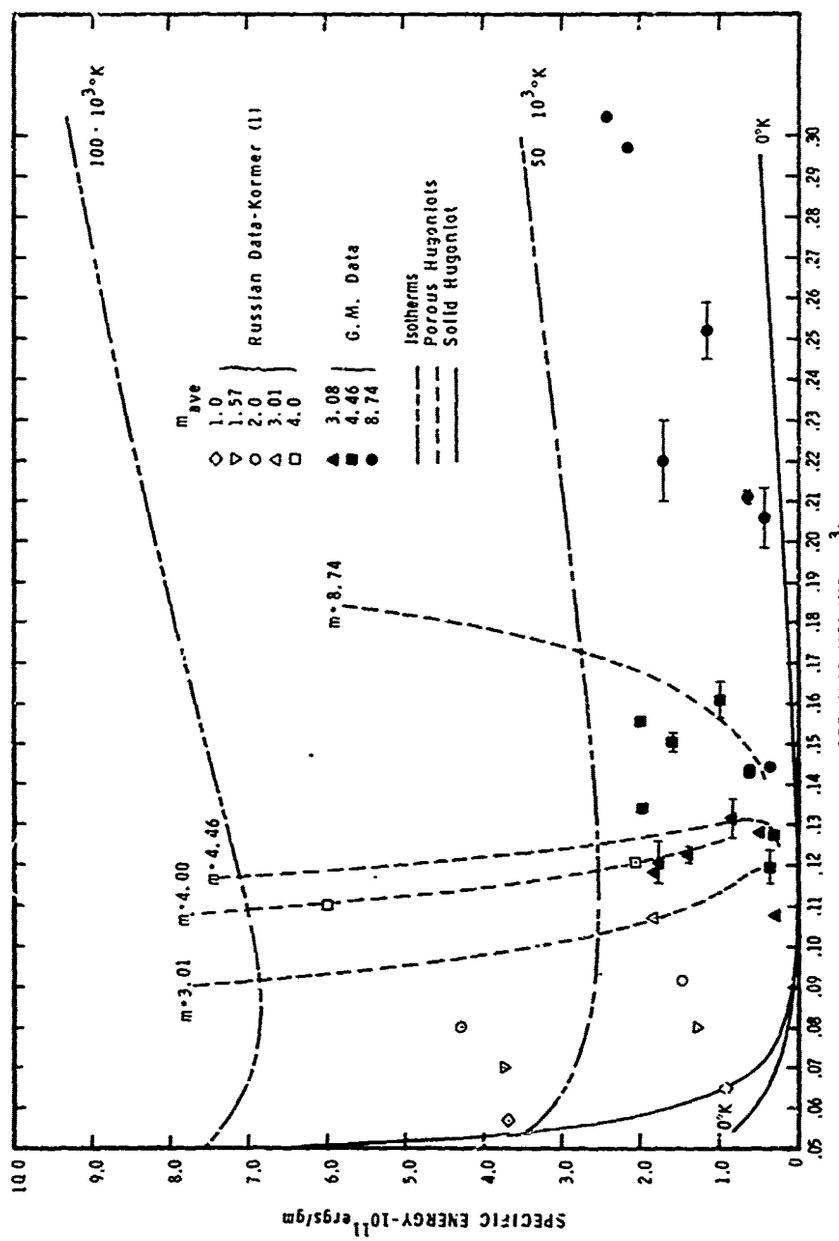

Figure 16 Specific Energy - Volume Diagram of Copper

records suggest this also. Event #3 in Figure 11 has been interpreted as the first arrival of a pressure pulse both because it represents a zone of extinguished light and because its time interval corresponds closely to that recorded by self-shorting pins. An additional implication suggested by the emitted light from Event #2 is that Event #3 is the arrival of a hot high velocity vapor or molten stream. The open cell structure of MetNet would probably allow fine streams to propagate several cell diameters before encountering further stationary solid material. The effect, however, of using the final wave or Event #4 as the stable equilibrated shock is to shift the P-V states so far that some states lie to the left of solid Hugoniot. Some precompression, then, must be occurring in the first wave, at least to the extent of modifying the initial specific volume an unknown and indeterminable amount. The optical records then invalidate the Hugoniot states determined by the simplistic pin experiments by destroying the assumption of shock state equilibrium and through lack of knowledge of the intermediate and final volume states.

In Figure 17 the time vs distance data from the optical records of step target impacts are presented. For all three distentions, the first wave is seen to parallel the second wave between the steps. Also, the waves appear to be decreasing in velocity with distance traveled. It is not possible to determine if this is due to an initial instability or if the waves are attenuating with distance. Finally, for the three distentions shown, the wave trajectories are similar for similar impact velocities.

It appears that the first wave and second wave, after establishing some separation, propagate at the same velocity. The separation of the two waves we interpret to be associated primarily with the cell size and, to some minor extent, the distentions.

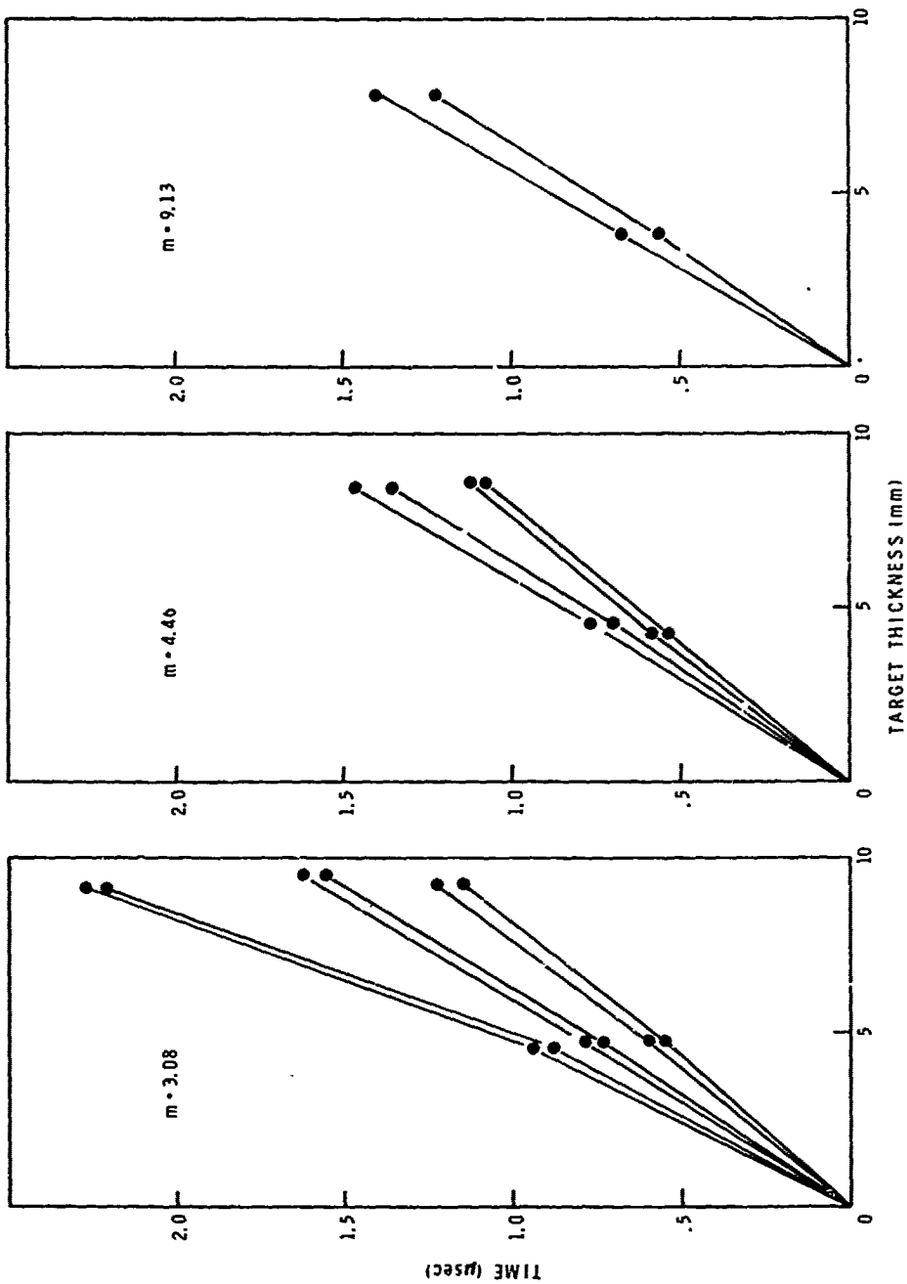

Figure 17 Shock Trajectories from Optical Data

If the waves are decreasing in velocity with distance, calculation of states at a point cannot be made solely on the knowledge of transit times.

The wave trajectories for the three distentions are similar for similar impact velocities as seen here and also as inferred from the wave velocities vs impact velocity as displayed in Figures 12, 13 and 14.

No other experimental techniques at these high pressure conditions have been reported which could have detected the existence of a double wave. This is particularly true if the leading wave carries sufficient energy as suggested in these experiments to significantly alter the stationary materials state. That this leading wave phenomenon is peculiar to materials such as MetNet is a moot point. It seems difficult to ignore the possibility of a ramped non-equilibrium wave even in finely powdered porous specimens with any significant distention.

SECTION V

CONCLUSIONS

On the basis of the experimental results described above, the following conclusions have been reached:

1. Optical observation of large distention, open celled copper, showed a multi-wave complex loading structure at high pressures.

2. There is some evidence that the waves in the distended copper are slowing down with distance of propagation. This is based on the data presented in Figures 6, 7 and 17. The wedge data showed variations in velocity of 1 to 3% at low pressures. The optical step data indicated a change in velocity between steps. This may be an initial instability or a continuous reduction of velocity with distance of propagation.

3. To a first approximation, the same wave speeds were observed in samples of different distentions for the same impact velocities.

4. Comparison of the results of the experiments with the predictions of the Russian equation of state is poor due to the multi-wave structure we observed.

In summary, the analysis of the experiments with porous copper show that the loading process cannot be represented as a simple shock process even at the highest pressures. A description of the process would have to include the cell size in addition to the porosity.

REFERENCES

1. Kormer, S. B., Funtikov, A. I., Urlin, V. D. and Kolensnikova, A. N., "Dynamic Compression of Porous Metals and the Equation of State with Variable Specific Heat at High Temperatures", Soviet Physics-JETP, Vol. 15, p. 477-488, 1962.

2. Kormer, S. B., Urlin, V. D. and Popuva, L. T., "Interpolation Equation of State and Its Application to Experimental Data on Impact Compression of Metals", Soviet Physics-Solid State, Vol. 3, p. 1547-1553, 1962.

3. Krupnikov, K. K., Brazhnik, M. I. and Krupnikova, V. P., "Shock Compression of Porous Tungsten", Soviet Physics-JETP, Vol. 15, No. 470, 1962.

4. Butcher, B. M., "Dynamic Crushup of Foams", SC-RR-66-325, Sandia Laboratory, Albuquerque, New Mexico, 1967.

5. McQueen, R. G., Marsh, S. P. and Carter, W. J., "The Determination of New Standards for Shock Wave Equation-of-State Work", Symposium High Dynamic Pressure, Paris, France, 1967.

6. Thouvenin, J., C. R. Acad. Sc.-Paris, France, Vol. 258, No. 3461, 1964.

7. Shipman, F. H., Isbell, W. M. and Jones, A. H., "High Pressure Hugoniot Measurements for Several Nevada Test Site Rocks", MSL-68-15, Manufacturing Development, Materials and Structures Laboratory, General Motors Technical Center, Warren, Michigan, March, 1968.

8. Isbell, W. M., Shipman, F. H. and Jones, A. H., "Hugoniot Equation of State Measurements for Eleven Materials to Five Megabars", MSL-68-13, Manufacturing Development, General Motors Technical Center, Warren, Michigan, December, 1968.

9. Jones, A. H., Isbell, W. M. and Maiden, C. J., "Measurement of the Very-High-Pressure Properties of Materials Using a Light-Gas Gun", J.A.P., Vol. 37, No. 9, p. 3493-3499, 1966.

10. Jones, A. H., Isbell, W. M., Shipman, F. H., Perkins, R. D., Green, S. J. and Maiden, C. J., "Material Properties Measurements for Selected Materials", MSL-68-9, Manufacturing Development, Materials and Structures Laboratory, General Motors Technical Center, Warren, Michigan, April, 1968.

11. Lyle, J. W., Schriever, R. L. and McMillan, A. R., "Dynamic Piezoresistive Coefficient of Manganin t\ 392 Kbar", J.A.P., Vol. 40, No. 10, p. 4663-4664, 1969.

APPENDIX

COMPUTER ROUTINE FOR THE EQUATION OF STATE WITH VARIABLE SPECIFIC HEAT

MSL-71-30

```
**                    POROUS MATERIALS EQUATION OF STATE PROGRAM
      DIMENSION V(50),S(50),PCOLD(50),ECOLD(50),PTL(50),ETL(50),
     1P1E(50),ETF(50),BETA(50),Z(50),CCK(50),GAM(50),     P(50),
     2ECAL(50),TMATL(5),HCOS(50),T(50),EHUG(50),CM(50),DPDV(50)
      COMMON A1,A2,A3,A4,A5,A6,A7
C
C
C
C     INPUT CONSTANTS
C         0 DEG. K SOLID DENSITY -                  RHOSO
C         DISTENTION -                              DM
C         SPECIFIC HEAT (V) -                       CV
C         SPECIFIC HEAT (P) -                       CP
C         INITIAL TEMPERATURE -                     T0
C         ELECTRON SPECIFIC HEAT -                  BETA0
C         ELECTRON TERM -                           G
C         7 MATERIAL CONSTANTS -                    A1 THRU A7
C         START VOLUME -                            VST
C         FINAL VOLUME -                            VFIN
C
C
      READ(5,10)(TMATL(I),I=1,5)
      READ(5,11)RHOSO,DM,CV,CP,T(1),BETO,G
      READ(5,11)A1,A2,A3,A4,A5,A6,A7
      READ(5,12)VST,VFIN
   10 FORMAT(5A4)
   11 FORMAT(7F10.5)
   12 FORMAT(2F10.5)
C
      DO 40 K=1,50
      L=9
      R=8.31432E+07/63.54
      P=12.0E+06
      TTK=100.
      VSO=1./RHOSO
      DELV=(VFIN-VST)/50.
      V(1)=VST
      S(1)=VSO/V(1)
      DO 100 I=2,50
      V(I)=V(I-1)+DELV
      S(I)=VSO/V(I)
      CALL ISOTH(VSO,S(I),PCOLD(I),ECOLD(I),GAM(I),DPDV(I))
      PCOLD(I)=PCOLD(I)*1.0E+12
      ECOLD(I)=ECOLD(I)*1.0E+12
      DPDV(I)=1.0E+12*DPDV(I)
      BETA(I)=BETO /(S(I)**G)
      CCK(I)= VSO*DPDV(I)
      IF(V(I)-.23)20,20,21
   20 Z(I)=L*R*T(K)/CCK(I)
      PTL(I)=(3.*GAM(I)+Z(I))*R*(T(K)-TTK)/((1.+Z(I))*V(I))
      ETL(I)=(2.+Z(I))*3.*R*(T(K)-TTK)/((1.+Z(I))*2.)
      GO TO 22
   21 PTL(I)=R*(T(K)-TTK)/V(I)
```

```
      ETL(I)=R*(T(K)-TTK)*3.0/2.
   22 CONTINUE
      HCOS(I)=COSH(BETA(I),T(K),B)
      PTE(I)=G*B**2/(BETA(I)*V(I))*ALOG(HCOS(I))
      ETE(I)=(B**2/BETA(I)      )*ALOG(HCOS(I))
      P(I)=PCOLD(I)+PTL(I)+PTE(I)
      ECAL(I)=ECOLD(I)+ETL(I)+ETE(I)
      EHUG(I)=.5*P(I)*(DM*VSO-V(I))
      CM(I)=(2.*ECAL(I)/P(I)-V(I))/VSO
      P(I)=P(I)*1.0E-06
      PCOLD(I)=PCOLD(I)*1.0E-06
      PTL(I)=PTL(I)*1.0E-06
      PTE(I)=PTE(I)*1.0E-06
  100 CONTINUE
      WRITE(6,13)(TYATL(I),I=1,5)
      WRITE(6,16)RHOSO,DM,CV,CP,T(K),BETO,G
      WRITE(6,17)
      DO 111 I=1,50
  111 WRITE(6,14)V(I),S(I),P(I),ECAL(I),PTL(I),ETL(I),PTE(I),ETE(I)
   18 FORMAT(1H 4E15.6)
      WRITE(6,7)(V(I),P(I),ECAL(I),EHUG(I), Z(I),I=1,50)
    7 FORMAT(1H ,5E15.6)
      T(K+1)=T(K)+10000.0
      CALL DATSW(0,ISW0)
      IF (ISW0-1)40 ,200,40
  200 WRITE(6,9)
    9 FORMAT(1H ,2(,12HSPEC. VOLUME,5X,10HSOUND VEL.,1X,14HINTERP. PAR...
     1,   //,5X,8HCM**3/GM,9X,6HCM/SEC,11X1HZ,//)
      DO 101 I=1,50
      CCK(I)=SQRT(CCK(I))
  101 WRITE(6,19)V(I),CCK(I),Z(I),DPDV(I)
      WRITE(6,15)(V(I),S(I),PCOLD(I),ECOLD(I),GAM(I),I=1,50)
   13 FORMAT(1H1,39HEQUATION OF STATE CALCULATIONS FOR - - ,5A4,//)
   14 FORMAT(1H ,8E15.6)
   15 FORMAT(1H1,23HISOTHERMAL STATE VALUES,//2X,12HSPEC. VOLUME,4X,
     111HCOMPRESSION,3X,13H     PRESSURE,4X,11H     ENERGY,//,6X,
     28HCM**3/GM,10X,4HV0/V,7X,8H    BARS,8X,7HERGS/GM,//(5E15.6))
   16 FORMAT(1H0,19HO DEG. K DENSITY = ,F10.5,5X,13HDISTENTION = ,F7.3,
     15X,20HSPECIFIC HEATS   V =,E15.6,2X,3HP =,E15.6,//
     2 5X, 15HINITIAL TEMP. =,F10.1,5X,25HINIT. ELEC. SPEC. HEAT = ,F10.
     3',5X,17HELEC.RON COEF. = ,F10.6,//)
   17 FORMAT(2X,
     112HSPEC. VOLUME,   4X,11HCOMPRESSION,3X,13HTOT. PRESSUR   ,11HTOT
     2. ENERGY,2X,13HLAT. PRESSURE,4X,11HLAT. ENERGY,1X,14HELEC. PRESSU
     3F,3X,
     412HELEC. ENERGY ,//6X,8HCM**3/GM,10X,4HV0/V,7X,8H    BARS,8X,7H
     5S/GM,11X,4HBARS,8X,7HERGS/GM,11X,4HBARS,8X,7HERGS/GM,//)
   40 CONTINUE
  201 CALL EXIT
      END
```